The Journal of Adhesion

ISSN: 0021-8464 (Print) 1545-5823 (Online) Journal homepage: www.tandfonline.com/journals/gadh20

Towards starch-based adhesives involving carbon dots as versatile crosslinkers

Valentin Silveira, Raffaello Papadakis & Stergios Adamopoulos

To cite this article: Valentin Silveira, Raffaello Papadakis & Stergios Adamopoulos (2025) Towards starch-based adhesives involving carbon dots as versatile crosslinkers, The Journal of Adhesion, 101:12, 1395-1421, DOI: 10.1080/00218464.2025.2464051

To link to this article: https://doi.org/10.1080/00218464.2025.2464051

THE JOURNAL OF ADHESION
2025, VOL. 101, NO. 12, 1395–1421
https://doi.org/10.1080/00218464.2025.2464051

Taylor & Francis
Taylor & Francis Group

Towards starch-based adhesives involving carbon dots as versatile crosslinkers

Valentin Silveira, Raffaello Papadakis, and Stergios Adamopoulos

Department of Forest Biomaterials and Technology, Swedish University of Agricultural Sciences, Uppsala, Sweden

ABSTRACT

In this study, biobased materials, Dialdehyde starch (DAS) and Carbon Dots (CDs) were synthesised to develop debondable adhesives via the formation of reversible imine networks between aldehyde and amine groups. Potato starch (St) was oxidised using Sodium periodate (NaIO4) and the modification was confirmed using FTIR spectroscopy, thermal analyses and Environmental scanning electron microscopy (ESEM). Two types of CDs were prepared: CD1, synthesized via a hydrothermal treatment of citric acid with formamide and aniline, and CD2, a post-functionalized version of CD1, prepared through a microwave-assisted reaction with polyethylenimine (PEI). CDs were characterized using XPS, fluorescence and absorbance spectroscopy, FTIR, TGA, DSC, as well as ESEM. DAS and CDs were reacted in DMAC to form DAS-CD conjugates through Schiff base formation. In the case of CD1, the reaction occurred through amino groups at the edges, while for CD2, the primary amino groups of PEI. The curing properties of these solutions with and without hexamethylenediamine (HMDA) as an auxiliary crosslinker were evaluated through ABES using beech veneer pressed at 160°C. Finally, debondability tests on veneer samples adhered with DAS-CD1 and DAS-CD2 were tested employing the reversibility of the Schiff-base connectivity motifs. Full debondability was achieved for DAS-CD1 after 1 hour in acidic solutions.

ARTICLE HISTORY
Received 9 December 2024
Accepted 2 February 2025

KEYWORDS
Carbon dots; starch; bio-based adhesives

1. Introduction

The development of bio-based adhesives is crucial for reducing environmental impact and decreasing dependence on petroleum resources.[1,2] Traditional petroleum-based adhesives contribute significantly to environmental pollution and are derived from non-renewable resources, which are becoming increasingly scarce. In contrast, bio-based adhesives are derived from renewable resources such as plants, which can be sustainably sourced and have a lower carbon footprint.[3,4] Moreover, bio-based adhesives often exhibit biodegradability, reducing the long-term environmental impact associated

CONTACT Raffaello Papadakis rafail.papadakis@slu.se Department of Forest Biomaterials and Technology, Swedish University of Agricultural Sciences, Vallvägen 9C, Uppsala 756 51, Sweden

with adhesive waste.[5] They also tend to be less toxic, making them safer for both human health and environment.[6] The shift towards bio-based adhesives aligns with the global sustainability goals and the principles of green chemistry, which emphasize the use of safer, renewable materials.[7] Recent advancements in the field have shown that bio-based adhesives can achieve performing characteristics comparable to their petroleum-based counterparts.[7]

Carbon dots (CDs) can play an important role in achieving this milestone due to their unique properties[8–10] and potential to enhance adhesive performance.[11–14] Indeed, the use of Carbon Dots as an additives for adhesive formulation has recently been explored in various ways. The versatility of carbon dots (CDs) has been explored as crosslinkers in bioadhesives, aiming to enhance drug delivery by increasing the porosity of gelatin-based gels while enabling optical tracking and photoactivated sterilization through their fluorescence.[15] Additionally, CDs have been investigated as crosslinkers in wood adhesives to improve the adhesion properties of conventional urea-formaldehyde (UF) adhesives.[12] By replacing hydrogen cohesive interactions within the UF resin with functionalized CDs (bearing amino, carboxyl, and hydroxyl groups), strong hydrogen bonds between the CDs and the polymer chains of UF can be achieved leading to enhancement of the original cross-linking structure and improvement of the micromechanical strength of bond lines.[12] Recent research also highlights the use of CDs as rigid nanofillers[11] to enhance energy dissipation and increase adhesive toughness, thereby improving resistance to failure. The surface functionalities of CDs, which provide excellent water dispersibility, make them a promising alternative to traditional nanofillers like silicon dioxide (SiO_2). Furthermore, the lower cytotoxicity of CDs has brought significant interest, and their fluorescence offers a valuable feature for routine safety checks during adhesive applications.

A wide variety of CDs derived from citric acid have been reported to date. Citric acid, a naturally occurring organic acid, is abundant, low-cost product, and exhibits excellent bioavailability and biocompatibility, making it an ideal precursor for CD synthesis[16,17] but also of novel bio-based adhesives.[18] Numerous CDs have been synthesized from citric acid, exhibiting high fluorescence quantum yields[19,20] and tunable photoluminescence, which are necessary for applications in energy conversion,[21] bioimaging,[22] sensing,[23] and optoelectronics. Additionally, citric acid derived CDs have been found to exhibit a corrosion inhibiting role[24] which is highly interesting for novel application in devices requiring high materials performance and endurance. Very interestingly, recent studies have demonstrated that citric acid-derived CDs can also significantly improve the performance of adhesives, showcasing their versatility.[12] Their incorporation into polysaccharide-based adhesives could enhance bonding strength and curing properties. In the context of wood adhesives, citric acid itself can play a crucial role. When

combined with starch, citric acid forms strong adhesive bonds through esterification and cross-linking reactions, improving adhesive properties and ensuring biodegradability and reducing toxicity.[25] As CDs often encompass moieties of their small-molecule precursors it is apparent that citric acid is a key ingredient for the development of CD-based adhesives.[15]

Embracing these findings, we report on the synthesis and post-functionalization of novel citric acid-derived CDs to enhance the curing properties of dialdehyde starch (DAS)-involving adhesives. Aiming to render them suitable for advanced adhesive formulations, we functionalized CDs with branched polyethyleneimine (PEI) to enhance crosslinking with dialdehyde starch (DAS). To improve the chemical stability and bonding of the intended adhesives, we developed a methodology that allows for the dynamic crosslinking of CDs with DAS in dimethylacetamide (DMAc) solvent. Additionally, we evaluated the need for an auxiliary crosslinker, hexamethylenediamine, to optimize adhesive performance. We applied mild conditions for curing and assessed the curing and bonding properties using the Automated Bond Evaluation System (ABES). To our knowledge, this approach has not been considered so far.

2. Results and discussion

2.1. Chemistry

For the needs of this study, carbon dots (CDs) were synthesized using citric acid, a bio-derived molecule widely recognized for its role in the development of graphene quantum dots and carbon dots.[26] Additionally, nitrogen-containing compounds (formamide and aniline) were employed to introduce N-doping into the CDs, delivering primary, secondary, or tertiary amino groups as well as corresponding amides. Similar synthetic approaches involving amines and citric acid have been recently reported.[27] This method was chosen to enhance the dipolarity of the CDs, thereby improving their dispersibility and solubility. Furthermore, these functionalities facilitate post-functionalization and crosslinking, which are crucial for developing novel adhesives. Specifically, CD1 was synthesized via a hydrothermal method using citric acid as the carbon source, along with significant amounts of formamide and aniline at 185°C (see Scheme 1).

After solvent removal following the hydrothermal process, CD1 was isolated and purified using size exclusion chromatography using Sephadex G-10, and eluted with MilliQ water. The collection criteria were based on the blue fluorescence of the desired CDs, monitored using a 365 nm UV-light source. The combined collected fractions were dried in a vacuum oven, yielding a yellow, shiny solid. This solid was then analyzed, and a portion of it was post-functionalized to product CD2. CD2 was synthesized via microwave

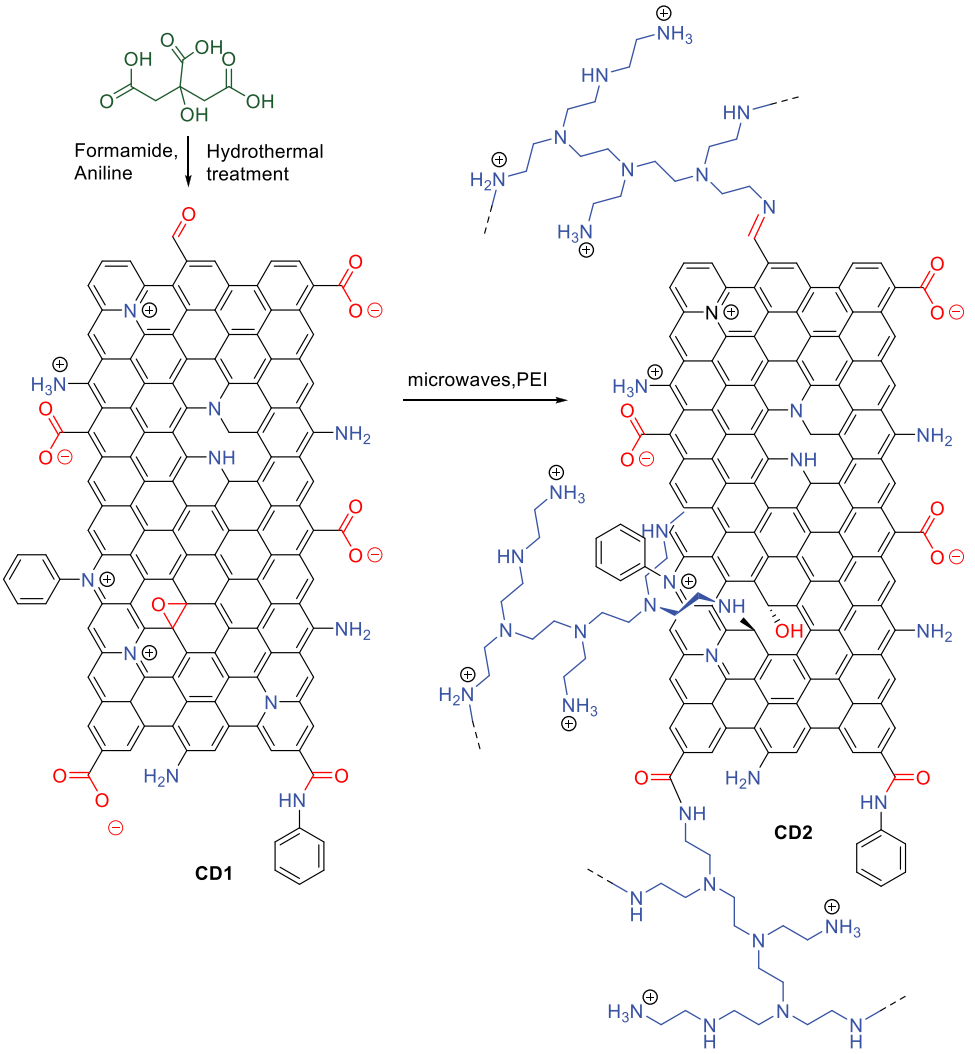

Scheme 1. The synthetic route used for the preparation of CD1 and CD2.

amidation of CD1 with branched polyethyleneimine (PEI). The synthesis was conducted in dimethylformamide (DMF), a solvent commonly used in similar microwave syntheses and proven to be effective for both CD1 and PEI. X-ray photoelectron spectroscopy (XPS) analysis suggests that further carbonization may have occurred during the post-functionalization process (*vide infra*). The proposed CDs have a quasi-spherical geometry (Figure 1) and a variety of functionalities as deduced through the different analytical methods used. Notably, connectivity motifs other than amide bonds might be present due to the occurrence of aldehyde or ketone functional groups appearing at the edges of the encompassed graphene layers in CD1 (see Scheme 1). While this model is mostly accepted by many research groups, a recent model developed by Boukhvalov et al. on the structure of carbon nanodots, which aligns with

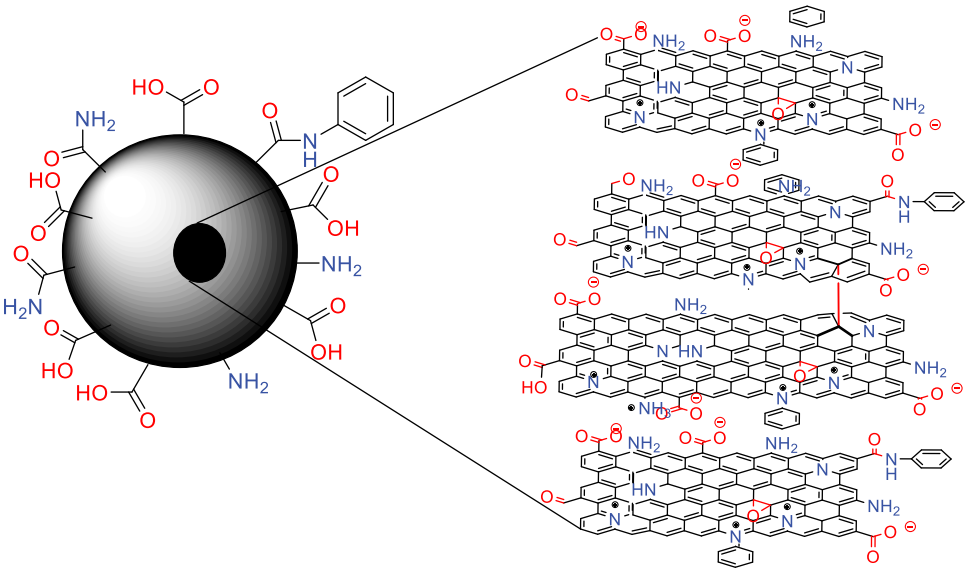

Figure 1. A schematic illustration of the spherical structure of CD1 with a hint of the structure of involved nano-graphene-like inner layers.

experimental observations (e.g. TEM studies) and is based on theoretical computations, suggests that CDs involve AA-stacked graphene layers with interlayer C – C covalent bonds and functional groups on their surface.[28] For instance, see the model in Figure 1, where the C – C interlayer bonds are marked in red.

Noteworthy, both CDs are very hygroscopic and they need to be stored under a dry atmosphere. While CD1 is readily soluble in water, CD2 becomes soluble only after heating above 50°C. Both CDs can be efficiently suspended in polar organic solvents such as DMSO, DMF, or DMAC.

The investigated adhesive formulations involve dialdehyde starch (DAS), a modified starch material prepared through the reaction of starch with sodium metaperiodate. This method was previously developed by our team.[29] We chose DAS as a key component of the adhesives due to its bioavailability (derived from starch) and its ability to undergo crosslinking with various crosslinkers such as amines, thanks to the presence of aldehyde groups. The DAS variant used in this study has been thoroughly analyzed (see Characterization) to fine-tune the reaction conditions, allowing for the optimal development of the DAS-CD adhesives.

For the development of the DAS-CD adhesives, a dynamic process was used involving condensation reactions between aldehyde units and the amino-groups of the two CDs (see Scheme 2). The role of such a dynamic conjugation methodology allowing for polysaccharide-graphene conjugations has been thoroughly discussed very recently.[30] In both cases (CD1 and CD2) CDs and DAS were suspended in DMAC and heated at 120°C overnight (16 h) with

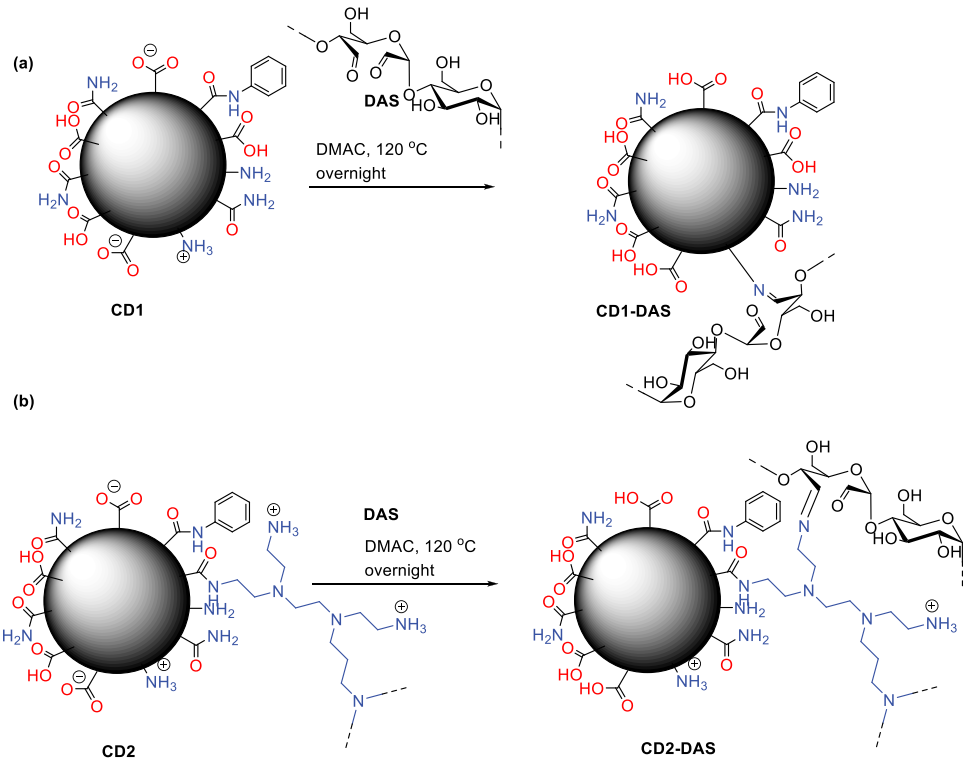

Scheme 2. Conjugation of CDs to DAS yielding CD1-DAS (a) and CD2-DAS (b).

CDs at 5% concentration relative to DAS. The dark brown solutions obtained using this process were used for ABES studies. As shown in Scheme 2, while conjugation of CD1 to DAS occurs through the amino-groups at its surface, in case of CD2, the corresponding Schiff base conjugation occurs through the primary NH_2 groups of the PEI units (which are covalently attached on CD2).

2.2. Characterization

2.2.1. X-ray photoelectron spectroscopy (XPS) analysis

X-ray photoelectron spectroscopy (XPS) is a surface-sensitive quantitative spectroscopic technique that can measure the topmost 200 atoms, (top 10 nm), of a surface. Given that the size of carbon dots (CDs) is typically less than 10 nm, XPS is a crucial technique for providing information on both the surface and the inner matter of a CD. In the case of CD1 and CD2, high-resolution (HR) C1s XPS spectra confirmed the presence of structures involving sp^2 and sp^3 hybridized carbon atoms, along with carbon atoms connected to nitrogen atoms (e.g., amines or amides) and distinct C=O bonding corresponding to the carboxylate and amide groups present in CD1 and CD2 (see Figure 2). The deconvolution of the measured HR-

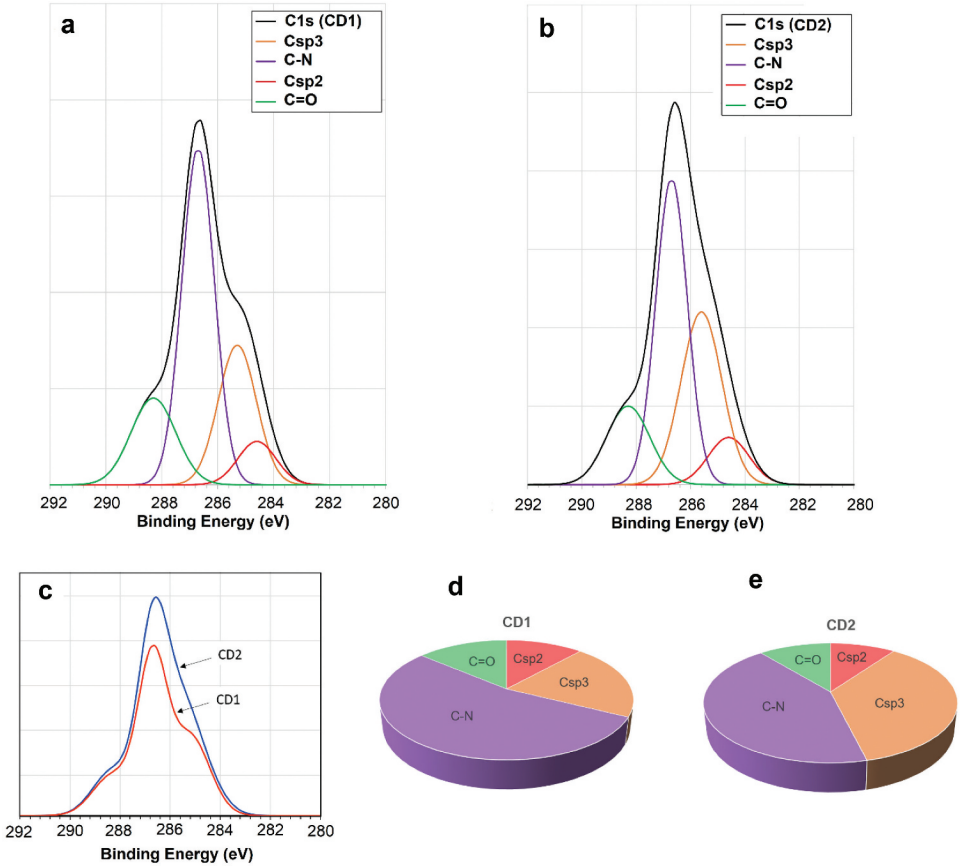

Figure 2. HR-C1s spectra of CD1 (a) and CD2 (b) and their deconvolution. (c) Superimposed HR-C1s XPS spectra of CD1 and CD2. Pie charts depicting the percentage contribution of each deconvolution signal in the HR-C1s XPS spectra of CD1 (D) and CD2 (E).

spectra for CD1 and CD2 revealed that, as expected, the post-functionalization of CD1 to CD2 resulted in enhanced C-N bonding (bands at 286.5 eV) due to the incorporation of PEI (a polyamine). It is noteworthy that CD1 has a substantial amount of N-involving groups (e.g. amides or amines) and this explains the large contribution of C-N bonding in the HR-C1s spectra of CD1 (more discussions on the types of groups in CD1 can be found in FTIR analysis below). This enhancement is evident from the significantly larger area of the C-N band in CD2 compared to CD1 (3.497 in CD1 and 3.897 in CD2; see Table 1 and Figure 2d,e). Additionally, the Csp3 signal (at 285.5 eV) increased after treatment with PEI. This increase aligns with the structure of branched PEI, which contains a large number of amino-methylene groups. Finally, distinct C=O bonding (broad bands at 288–288.5 eV) was identified through the HR-C1s spectra of both CDs examined. These bands are attributed to the presence of carboxylates, amides, or esters (all involving C=O bonds). Interestingly,

Table 1. Integrals and percentage contribution of the four deconvoluted signals of the HR-C1s and N1s XPS spectra of CD1 and CD2.

		CD1		CD2	
Signal	Band Energy (eV)	Integral	Percentage	Integral	Percentage
Csp2	285.0	0.759	11.7	0.899	9.9
Csp3	285.5	1.349	20.7	3.297	36.3
C-N	286.5	3.497	53.8	3.897	42.9
C=O	288.0–288.5	0.899	13.8	0.999	10.9
graphitic N	398.0–398.3	0.245	7.09	0.244	5.33
pyrrolic N	399.9–400.1	1.365	39.5	1.621	35.4
$-NH_3^+$	401.9–402.0	1.848	53.4	2.710	59.2

the C=O signal increased somewhat in the case of CD2 (see Table 1), presumably due to further carbonization and oxidation occurring under the microwave conditions applied to CD1.

The above small but important changes in the XPS of CD2 produced after the post-functionalization of CD1, lead to important changes in the shape and intensity of the spectra (see Figure 2 for comparison). The presence of PEI functionalities in CD2 is further supported through the FTIR analyses (*vide infra*).

Additional evidence of the introduction of PEI *via* condensation (amidation) on the surface of CD1 can be provided through a comparison of the High Resolution N1s-XPS of CD1 and CD2. The splitting of the various convoluted bands in this case allows for a better comparison due to the lower uncertainty upon deconvolution. As seen in Figure 3 (Panels A and B), a drastic increase of the band centered at 402 eV corresponding to $-NH_3^+$ groups is observed[31] in the N1s-XPS of CD2, corresponding to 59.2% of the entire convoluted N1s-XPS peak. At this level, the aforementioned band results in clear peak splitting. The corresponding contribution of this band in the N1s-XPS of CD1 was 53.4%, i.e., approximately 6% lower (Figure 3d and Table 1). Noteworthy, amino/ammonium groups are also present in CD1 since aniline was used in its hydrothermal production as an N-doping agent. The described finding is clear evidence of the introduction of PEI functionalities onto the CDs. Moreover, upon treatment of CD1 with PEI, the pyrrolic-N[32] and graphitic-N[32] content is retained at nearly the same levels (35–39% and 5.3–7.0%, respectively). The lowering of contribution of these peaks in CD2 is presumably associated with a "dilution effect" after the introduction of the PEI functionalities. Moreover, it also indicates that no drastic changes are observed on the CDs core upon treatment with PEI.

2.2.2. FTIR Analysis

2.2.2.1. CD1 and CD2. The complex FTIR spectrum of CD1 exhibits numerous signals attributed to the incorporation of a variety of functional groups in the structure. Most important is the presence of amide groups, with a sharp, strong signal at 1697 cm^{-1} corresponding to a typical C=O stretching band, as

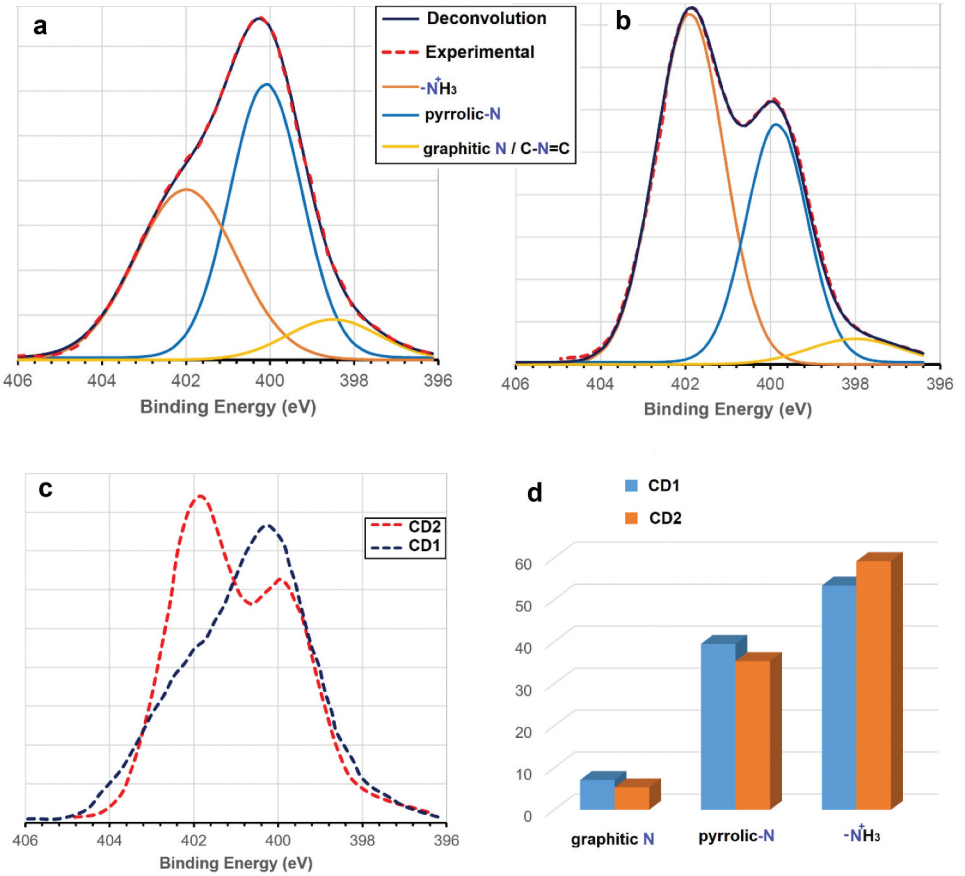

Figure 3. HR-N1s spectra of CD1 (a) and CD2 (b) and their deconvolution. (c) Superimposed HR-N1s XPS spectra of CD1 and CD2. Bar diagram depicting the percentage contribution of each deconvolution signal in the HR-N1s XPS spectra of CD1 (d).

well as carboxylate functionalities with symmetric C=O stretching bands at 1345 and 1399 cm^{-1}. Evidence of the presence of pyridinic nitrogen atoms (N-doping) is based on a signal centered at 1497 cm^{-1}. Additionally, CD1 involves amino groups with a distinct stretching N-H band at 3379 cm^{-1} and possibly N-H amine bending at 1635 cm^{-1}. The presence of aliphatic (sp^3 hybridized carbon; see also XPS analysis) is also apparent in a convoluted broadband with elements of peaks at 2928 and 2867 cm^{-1}, corresponding to the asymmetric stretching of C-H bonds in aliphatic chains. Additionally, aromatic amine-related functionalities are present (derived from aniline) with N-H stretching at 3379 cm^{-1} and convoluted aromatic C-H (phenyl rings) stretching bands around 3100–3000 cm^{-1}, and finally, aromatic C-H bending between 900–700 cm^{-1} (specifically at 884, 781, and 734 cm^{-1}).

On the other hand, the FTIR spectrum of CD2 indicated many similarities with that of its parent CD1. The spectrum exhibits various bands attributed to the incorporation of PEI in the CDs via amidation, the most important being

the N-H stretching broad band around 3366 cm^{-1}, indicative of N-H stretching vibrations from primary and secondary amines (see Figure 4). The C-H stretching peaks at 2858 and 2931 cm^{-1} correspond to the C-H stretching vibrations from the aliphatic chains of PEI. Additionally, N-H bending bands are present, such as a strong band at 1566 cm^{-1} and other convoluted bands between 1560 and Various C-N stretching bands are also observed between 1000 and 1300 cm^{-1}, for example, at 1074, 1136, and 1192 cm^{-1}, attributed to C-N stretching vibrations. The amide signals are also present in the spectra of CD2 as in CD1, specifically a strong sharp band at 1698 cm^{-1} (also present in CD1 at 1697 cm^{-1}; vide supra) and possibly other convoluted bands between 1640 and 1700 cm^{-1} at lower wavenumbers than the main peak at 1697 cm^{-1}. It is important to mention that the characteristic structures presented in Scheme 1 are mostly based on the findings of the XPS and FTIR analyses discussed above. 1600 cm^{-1}, which are associated with N-H bending vibrations.

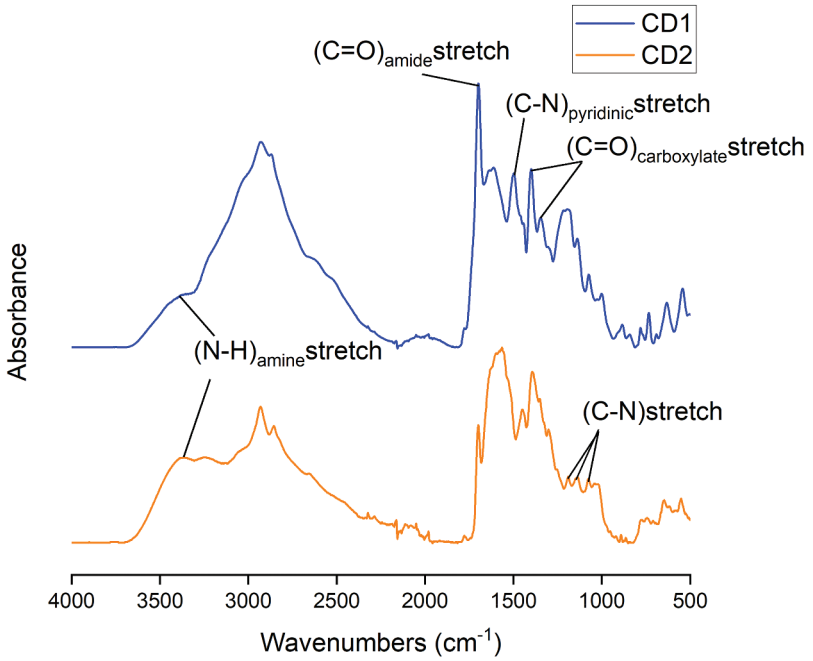

Figure 4. FTIR spectra of solid samples of CD1 and CD2.

2.2.2.2. Dialdehyde starch. The FTIR spectra show significant differences between DAS and Potato Starch (St), particularly in the carbonyl region and the 500–1000 cm^{-1} range. Specifically, the DAS spectrum exhibits peaks around 1729 cm^{-1} and 1679 cm^{-1}, associated with the carbonyl (C=O) stretching vibrations. These peaks are not present in the FTIR spectra of native St. The FTIR spectra of St (Figure 5) on the other hand showed three characteristic peaks at 990, 1075, and 1150 cm^{-1}, attributed to C-O bond stretching.

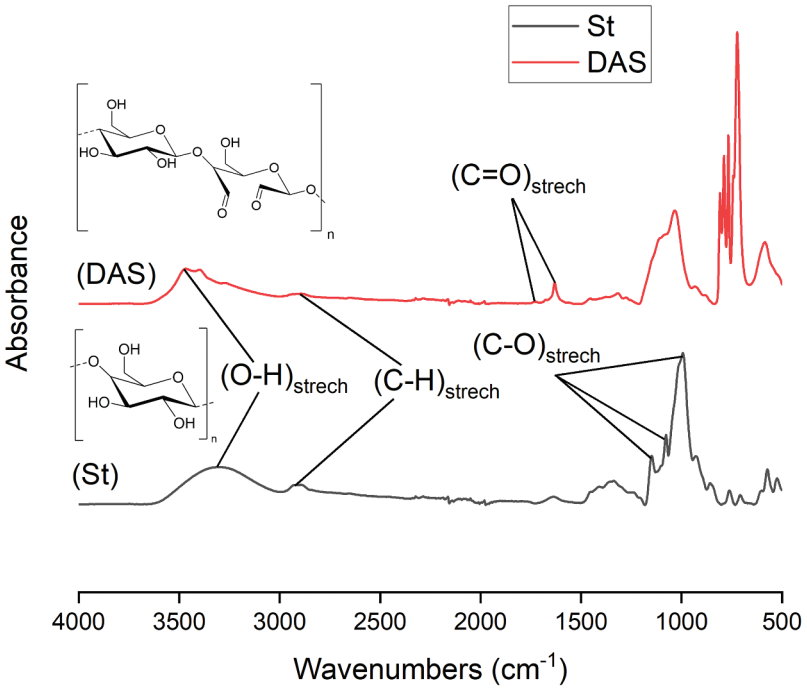

Figure 5. FTIR spectra of solid samples of DAS and St.

These peaks disappeared in the DAS samples after oxidation.[26] The absorption peaks in case of St at 1640 and 3290 cm^{-1} could be related to trapped moisture in the non-crystalline region of the starch structure or intermolecular hydrogen bonds.[26] Additionally, The peak at 2960 cm^{-1} in case of St assigned to CH group stretching, shifted slightly to 2880 cm^{-1} within the 2800–3000 cm^{-1} range, after the oxidation of St to DAS. Moreover, the DAS samples displayed a new stretching vibration at 1729 cm^{-1}, associated with carbonyl groups and a peak at 875 cm^{-1}, indicating hemiacetal bonds between dialdehyde groups and adjacent hydroxyl groups. The decrease of the intensity of the peak corresponding to hydroxyl groups around 3400 cm^{-1} corroborate the consumption of these latter toward the formation of aldehyde groups.

2.2.3. Spectrophotometric evaluation of the CDs

A clear proof of the formation of the CDs is provided through their measured emission properties. Both CDs emit light in an excitation dependent fashion (see Figure 7).[33,34] CD1 appears to be more emissive than CD2 when their emission properties are examined in aqueous solutions with about the same concentration. This is presumably associated with the presence of PEI units in case of CD2. The surface states responsible for CD-emission are drastically dependent on dopants, functional groups (especially bulky ones e.g. polymeric species).

The maximal emission in both cases is observed upon excitation at approx. 327 nm (near UV-light). Interestingly, CD2 exhibits some emission also in the visible region at around 620 nm as a result of a weak absorption band of CD2 at roughly 590 nm (see Figure 6). This absorption is clearly associated with the presence of PEI and accumulation of different unsaturated connectivity motifs e.g. imine (Schiff bases).

2.2.4. Thermal analysis

To be suitable for wood adhesive applications, CDs and DAS must exhibit thermal stability within the temperature range used in these processes. In this study, the temperature was set to 160°C. The thermal stability of the different materials was assessed using thermogravimetric (TG) and derivative thermogravimetric (DTG) analysis.

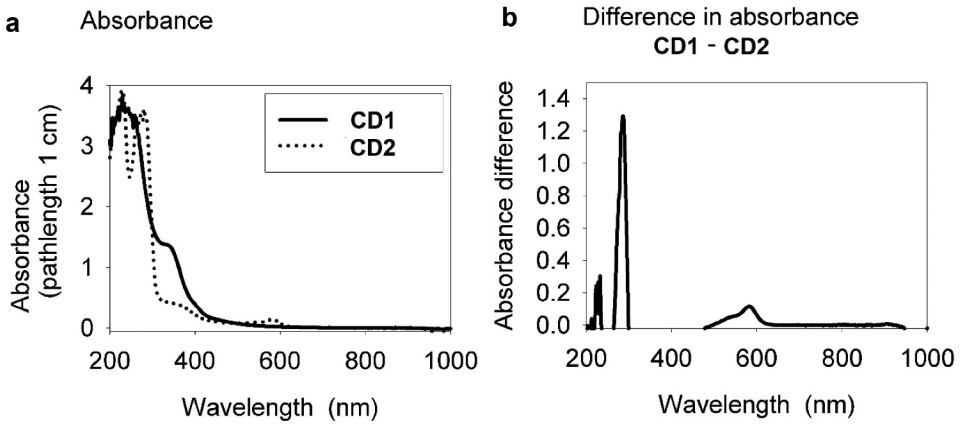

Figure 6. Absorption spectra of CD1 and CD2 (a) and difference in absorbance of CD1 and CD2 (b).

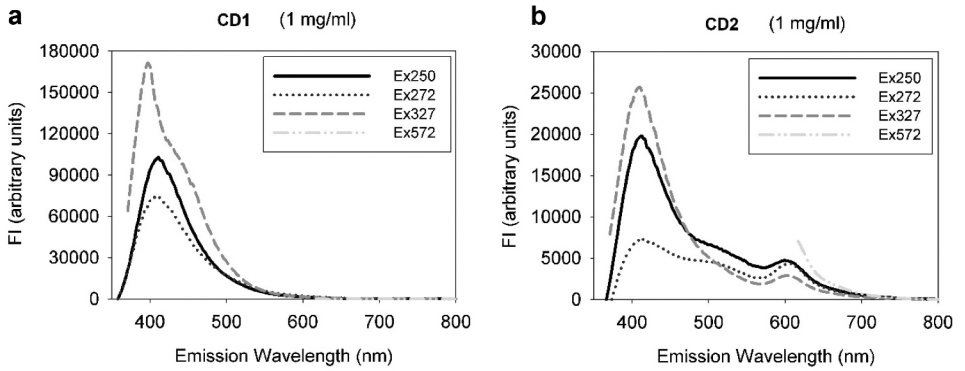

Figure 7. Emission spectra when dissolved in water at concentration 1mg/mL upon excitation at various wavelengths for CD1 (a) and CD2 (b).

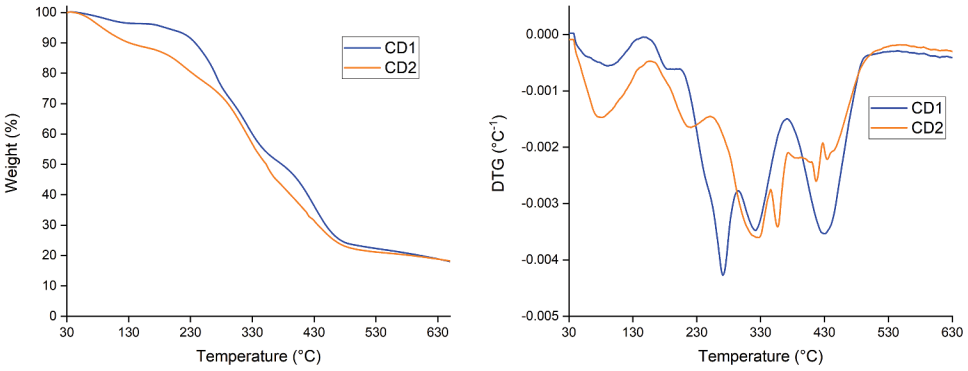

Figure 8. TG (left) and DTG (right) analyses of CD1 and CD2.

The TG and DTG analyses of the two CDs revealed that both are relatively stable up to temperatures close to 150°C (see Figure 8). The mass losses up to this temperature mostly correspond to the loss of trapped water. The TGA profiles of CD1 and CD2 are very similar, yet DTG indicates a range of thermal decomposition processes occurring at elevated temperatures (>200°C). Due to the high polydispersity of the CDs and the large range of encompassed functional groups, it is challenging to understand their multi-step thermal decomposition pathways at temperatures higher than 200°C. Generally, TGA results can be ambiguous when there are more than two peaks, as these peaks cannot be straightforwardly attributed to surface and core decomposition based solely on the temperature.[35] Nonetheless, for the scope of this work, their thermal behavior up to 160°C (the set temperature for the curing tests) indicates that both CDs are a good match for the design of resins/adhesives involving these CDs and DAS.

On the other hand, the thermograms of unmodified (St) and oxidized (DAS) (Figure 9) show fewer degradation steps. Unmodified starch displayed a two-step mass loss: the first at 100°C corresponds to approximately 5% mass

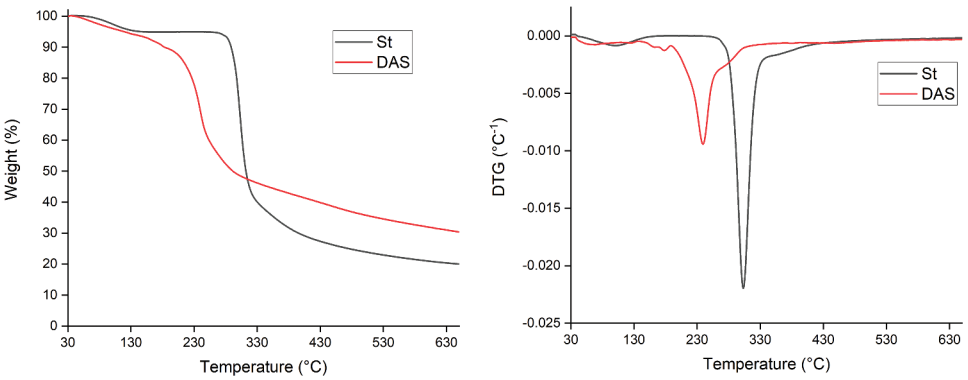

Figure 9. TG (left) and DTG (right) analyses of DAS and parent starch (St) material.

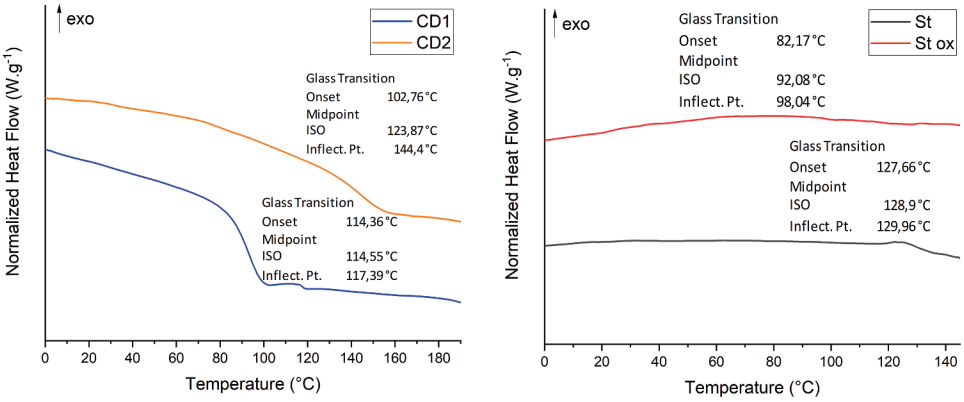

Figure 10. DSC analyses of CDs CD1 and CD2 (left panel) and of DAS and native St material (right panel).

loss of the water trapped in the starch structure. The second, occurring around 320°C is associated with the starch backbone thermal degradation, with an onset temperature of 205°C and a peak weight loss at 302°C. The residual weight was approximately 20%. The oxidized starch also displayed a two-step mass loss that can be interpreted in a similar way to native starch. However, the step corresponding to the starch degradation appeared at a lower temperature and started around 175°C with a peak weight loss at 240°C according to the DTG thermograms. It can be explained according to previous work[36] as the oxidation of starch results in the depolymerization of amylose and amylopectin chains, leading to a reduction in molecular weight and, consequently, a decrease in the thermal stability of starch. Moreover, it was reported that[37] Dialdehyde starch exhibits lower thermal stability compared to native starch, primarily due to the cleavage of the C2–C3 bonds in glucosyl units and the breaking of glycosidic bonds in the starch backbone.

Figure 10 shows the Differential scanning calorimetry (DSC) thermographs of CD and starch samples.

Both CDs exhibit glass transition temperatures (Tg) higher than 100°C, with CD2 showing a slightly higher Tg than CD1 (124°C vs. 115°C). CD2, with its higher Tg, is expected to exhibit slightly better mechanical properties after processing (thermal pressing at 160°C) compared to CD1. This could translate to slightly better performance in terms of rigidity and resistance to deformation under stress. Overall, the higher Tg of CD2 suggests a wider processing window, making it potentially more versatile and easier to handle during the adhesive formulation process. In terms of potential adhesive performance, both CDs are expected to perform well, with CD2 offering a slight edge in thermal and mechanical stability compared to CD1. The slightly higher Tg of CD2 can be explained by the restricted molecular mobility in CD2 compared to CD1. This restriction is due to pronounced H-bonding in CD2, attributed

to the presence of PEI units, which limits the mobility of polymer chains. Consequently, more energy (higher temperature) is required to achieve the molecular motion associated with the glass transition. Additionally, intermolecular interactions are more pronounced in CD2 due to H-bonding, contributing to the overall intermolecular forces within the material and generally leading to higher Tg values. Overall, both CDs are suitable for use at 160°C, but CD2 may provide marginally better performance due to its higher Tg.

On the other hand, the native potato starch displayed a Glass transition temperature of around 129°C. The Tg of unmodified starch was determined to be around 129°C. Previous research[38] has highlighted the significant influence of moisture content on the Tg of starch. Consequently, a lower moisture content of starch leads to higher Tg values compared to those reported in other studies. The oxidized starch showed a Tg around 92°C, this decreased value cannot be attributed to a different moisture content as the TGA analysis previously showed (see Figure 9) a similar moisture content of 5% for both starch. The significant decrease in Tg can be attributed to the formation of aldehydes during oxidation, which increases polymer mobility by reducing the number of hydroxyl groups and consequently weakening hydrogen bonding.[39]

2.2.5. Analysis of the morphology

2.2.5.1. Scanning electron microscopy (SEM) analysis of CD1 and CD2. CD1 (Figures 11a,b): The SEM images of CD1 reveal quasi-spherical particles with some of them merged to one another in varying sizes and relatively smooth textures. Similar morphologies have recently been reported for different CDs.[40,41] In Figure 11a, the particles are loosely aggregated and irregularly distributed across the field of view, with a scale marker at 100 µm. In contrast, Figure 11b which is an image realised at higher magnification (a scale marker of 50 µm) shows more distinct and larger quasi-spherical particles that are uniformly distributed, with smoother surfaces. The quasi-spherical shape and smooth surface of these particles is in line with the freeze-drying process[42] used for their fabrication which promotes spherical morphology.

CD2 (Figures 11c,d): The SEM images of CD2 depict densely packed, flake-like structures. Figure 11c shows these flakes arranged in a compact and possibly crystalline structure, with sharp, well-defined edges at a scale 20 µm. Figure 11d provides a closer view of a single flake-like structure, revealing its detailed geometry with smooth faces and sharp edges. The scale marker of 5 µm allows for a close examination of the flake's surface and edges, suggesting a high degree of regularity and precision in its formation. The flake-like morphology indicates a different formation process, such as exfoliation or layer-by-layer assembly, resulting in distinct layered and sharp-edged structures.

These morphological differences between CD1 and CD2 can significantly influence their properties and potential applications, with CD1's

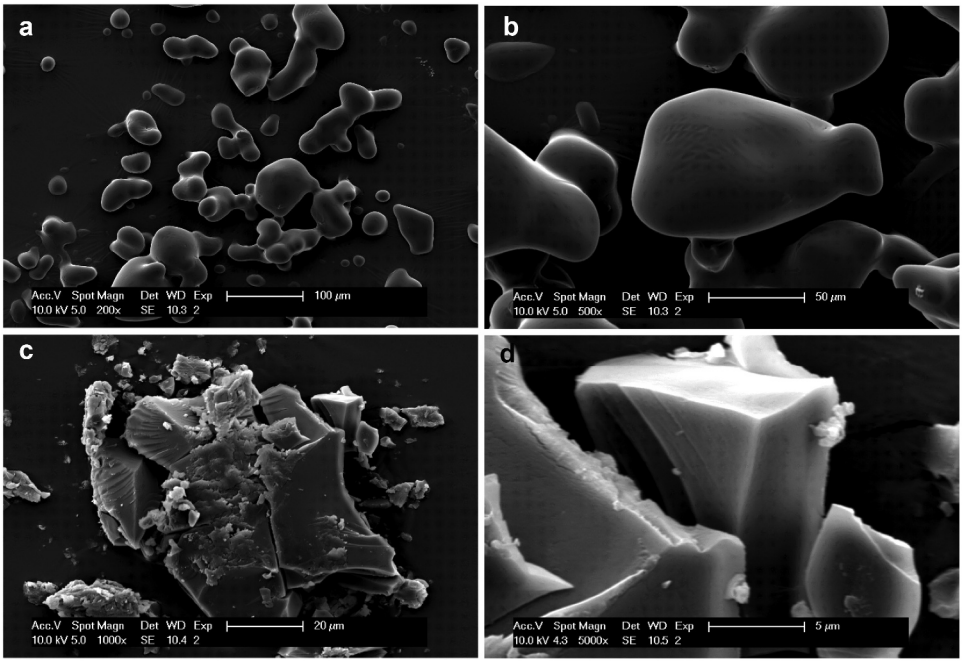

Figure 11. Scanning electron microscope (SEM) images of CD1 (a-b) and of CD2 (c-d).

quasi-spherical particles being suitable for applications requiring smooth, spherical morphologies, and CD2's flake-like structures being ideal for a wide range of adhesive applications needing layered, crystalline-like materials.

2.2.5.2. Scanning electron microscopy (SEM) analysis of DAS. The SEM images of Dialdehyde Starch (DAS) at 150× magnification (Figure 12a) reveal individual particles with a rough texture scattered across the field. At 1500× magnification (Figure 12b), a cluster of particles with more defined edges and intricate surface details, including tubular structures, is visible. These images illustrate a clear difference between DAS and the parent starch material (seen in Figure 12c,d), which exhibits smooth, oval to round-shaped particles densely packed together, a typical morphology encountered in starch. This drastic morphological change (which has been reported before upon oxidation of starch[43]) can significantly influence the miscibility and reactivity of DAS in the intended adhesive formulations (DAS-CD1 and DAS-CD2).

2.2.6. Adhesive bond strength development evaluation using ABES

2.2.6.1. Influence of pressing time. Pressing time is a critical factor as it influences bond strength, production speed, and energy consumption. To assess its impact on bonding strength, tests were conducted at a fixed pressing

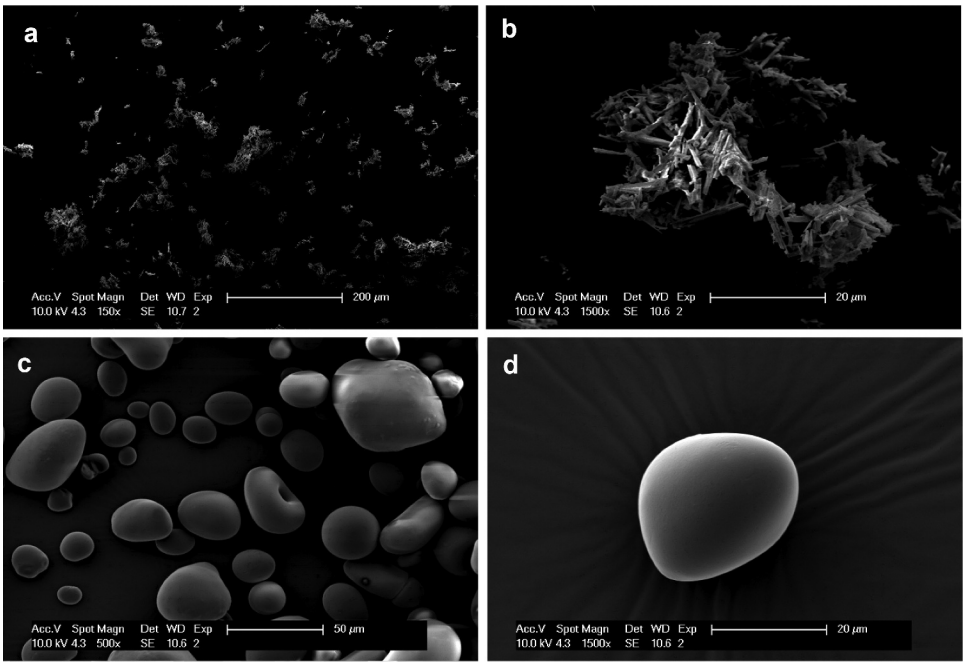

Figure 12. Scanning electron microscope (SEM) images of DAS (a-b) and of starch (c-d).

temperature of 160°C using the ABES system depicted in Figure 13. As anticipated, the results indicate that extended pressing times result in greater shear strength due to improved curing and solvent loss of the adhesives. This finding aligns with the observations of previous studies, which reported that longer pressing times enhance adhesive bonding, thereby increasing bond strength.[44]

2.2.6.2. Influence of HMDA. The prepared adhesive consists of a mix of linear and branched chains from DAS and Hexamethylenediamine (HMDA). The curing process is driven by the evaporation of the solvent (DMAc) and the cross-linking between the aldehyde groups of DAS and the amino groups of HMDA, resulting in the formation of imines. The internal cohesion is due to the formation of this imine network, while adhesion might be explained by the interlocking of starch chains in the wood structure and hydrogen bonding between hydroxyl groups from DAS, amino groups from HMDA, and hydroxyl groups present in the different components of wood (lignin, hemicellulose, cellulose).

As seen in Figures 14 and 15, solutions containing only DAS or only HMDA show adhesion with respective maximum shear strengths of 2.40 MPa ±0.11 and 2.95 MPa ±0.12. The formation of the imine network improves the bonding strength of DAS, achieving a maximum average shear strength of 3.63 MPa ±0.44.

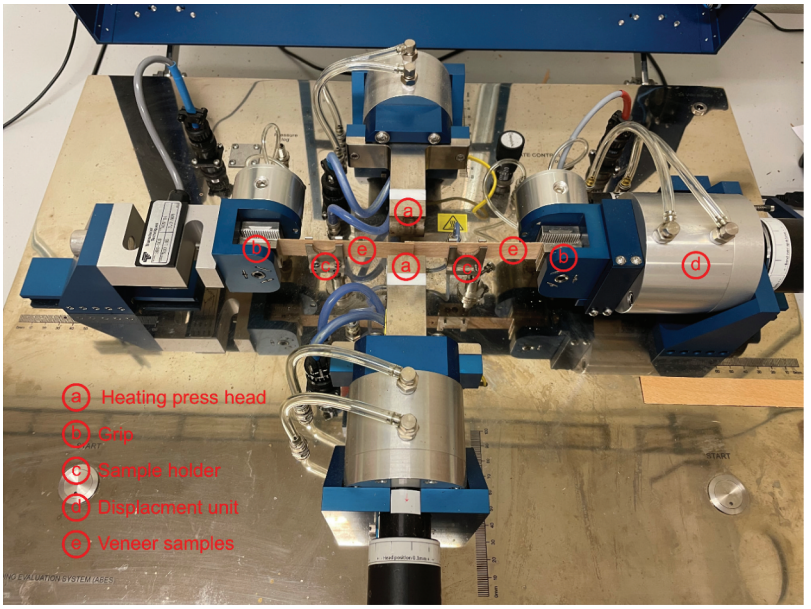

Figure 13. Top view of the ABES equipment used in this study.

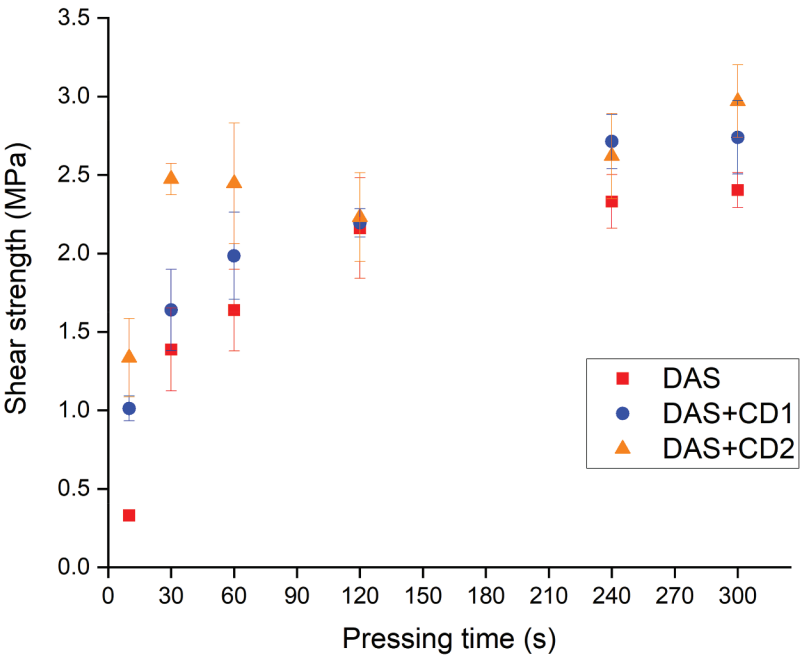

Figure 14. Plots of shear strength as a function of pressing time (at set temperature 160°C) for DAS, DAS+CD1 and DAS+CD2.

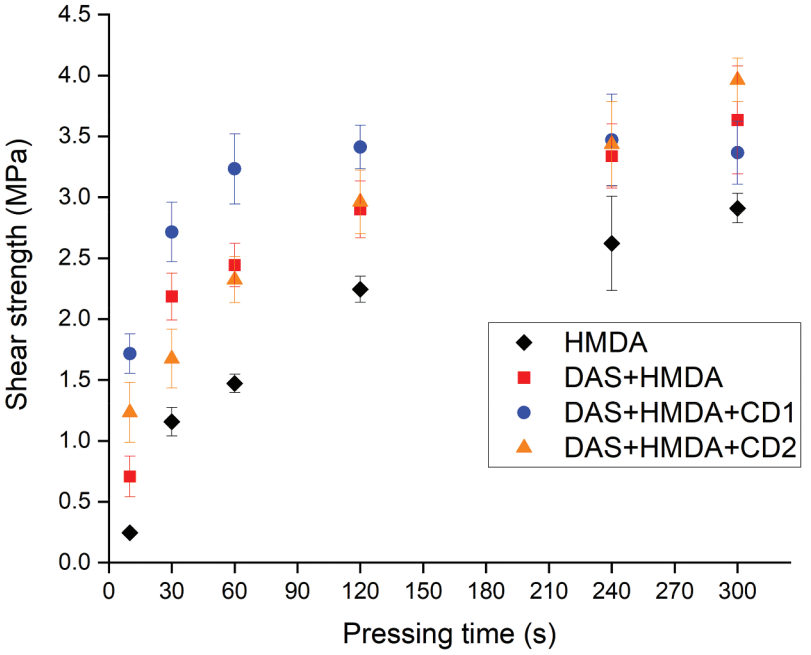

Figure 15. Plots of shear strength as a function of pressing time (at set temperature 160°C) for HMDA, DAS+HMDA, DAS+HMDA+CD1 and DAS+HMDA+CD2.

2.2.6.3. Influence of carbon dots. Figure 14 shows the evolution of shear strength over pressing time for Dialdehyde starch solution in the presence or not of the different synthetized Carbon dots. The Solution containing only DAS shows a continuous increase of shear strength over time reaching a maximum at around 240s with 2.3MPa ±0,17. The solutions containing CDs show faster curing, reaching the maximum shear strength of DAS solution at only 30s for CD2 with 2.47MPa ±0,10 and 120s for CD1 with 2.19MPa ±0,09. We believe that the amino groups present on both Carbon dots lead to the crosslinking of DAS enabling a better compatibility between the two materials. However, the amino groups of PEI grafted on CD2 might be more accessible due to the carbon chain length thus more reactive, improving the crosslinking between starch and CD2 compared to CD1. Moreover, in the presence of HMDA, we can observe a reverse trend, indeed, CD1 shows faster curing than CD2. We believe that this is due to the fact that the dialdehyde starch that has reacted with CD2 has less available reactive aldehyde than the one that as been crosslinked with CD1 allowing in a first step HMDA to crosslink more DAS+CD1 than DAS+CD2. However, after 300s we believe that the more hindered aldehyde present on DAS+CD2 is given enough time to react resulting in a higher shear strength of 3.96MPa ±0,18.

2.2.6.4. Reversibility test. The imine formation is known to be a reversible reaction.[45] Indeed, at acidic pH the imine can be hydrolysed leading back to

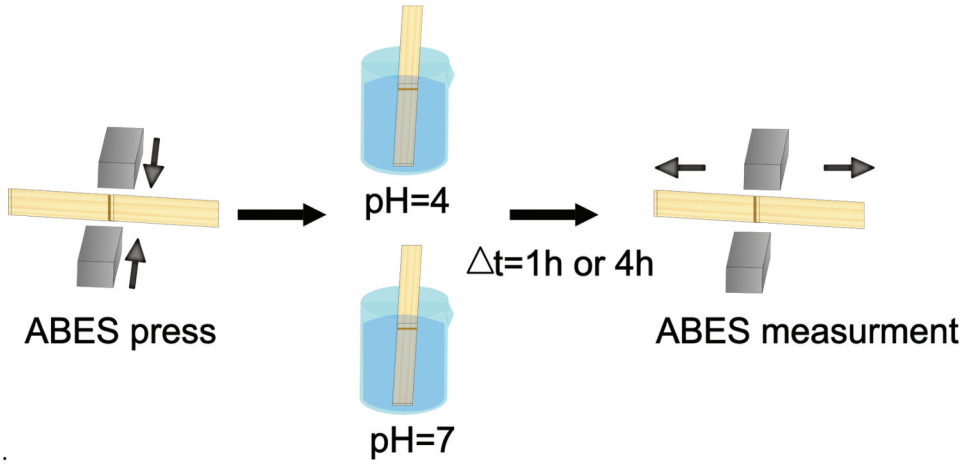

.

Figure 16. Illustration depicting the procedure followed for the reversibility tests on veneers adhered with resins **DAS+HMDA**, **DAS+HMDA+CD** (1 or 2).

Table 2. ABES results obtained after reversibility test performed at pH 4.

pH =4		
Time (h)	Average Maximum shear strength (Mpa)	Resin
1	1.49±0.21	DAS+HMDA
1	0	DAS+HMDA+CD1
1	1.06±0.05	DAS+HMDA+CD2
4	1.50±0.17	DAS+HMDA
4	0	DAS+HMDA+CD1
4	1.27±0.15	DAS+HMDA+CD2

the formation of amine and aldehyde. We expect that this will enable the adhesive to debond on demand in the presence of acidic conditions. The bond strength of veneer bonded with DAS+HMDA, DAS+HMDA+CD1 and DAS +HMDA+CD2 was then recorded using ABES after immersion in neutral water solution and acidic water solution. If in general the shear strength decreased after immersion in both solutions, only DAS+HMDA+CD1 was completely debonded after 1hour in an acidic solution (see Figure 16). Indeed, DAS+HMDA+CD2 will still show an average shear strength of 1.27MPa after 4 hours in acidic against 1.81MPa in neutral solution (detailed results are gathered in Tables 2 and 3). We believe this might be the result of the PEI chain making the system more water-resistant compared to CD1.

2.3. Experimental section

2.3.1. Materials

Citric acid monohydrate, aniline, formamide (FA), N,N-dimethylformamide (DMF), N,N-dimethylacetamide (DMAc), 1,6-Hexanediamine (HMDA), Sodium periodate (NaIO4), all of reagent grade were purchased from Sigma

Table 3. ABES results obtained after reversibility test performed at pH 7.

pH =7		
Time (h)	Average Maximum shear strength (Mpa)	Adhesive
1	1.95±0.21	DAS+HMDA
1	0.71±0.05	DAS+HMDA+CD1
1	2.11±0.20	DAS+HMDA+CD2
4	1.64±0.36	DAS+HMDA
4	0	DAS+HMDA+CD1
4	1.81±0.13	DAS+HMDA+CD2

Aldrich. Branched polyethylenimine (PEI) (average Mw ~ 25,000) and Potato Starch were also purchased from Sigma Aldrich. Purified water used in this research was produced using a Milli-Q® water purification system (Millipore). Beech veneer samples were cut at dimensions: 170 mm x 20 mm. For microwave treatment, a household microwave oven operating at scalable power with a maximal 900 MW power was used. Microwave reactions were carried out in Biotage 352,016 microwave reaction vials. Sephadex G-10 and G-25 (Medium) were purchased from Cytiva.

2.3.2. Synthesis

Carbon dots CD1 were synthesized using the following hydrothermal method. Citric acid (2.00 g) was wetted with 1.00 g of formamide and then 1 g of freshly distilled aniline (1.00 g) was added. The slurry was mechanically treated in a mortar and finally dissolved in 25 mL of MilliQ water. Subsequently, the solution was heated at 185°C for 24 h in a 50.0 mL Teflon-lined autoclave. After this process, the reaction mixture was transferred in a 100 mL round bottom flask (rbf) and the solvent was removed using rotary evaporation. The obtained dark orange product was purified through size exclusion chromatography (Sephadex G-10) to remove unreacted reagents and low molecular weight impurities. After this procedure, the obtained dialyzed sample was freeze-dried to obtain a fluffy deep-yellow colored powder. Final yield: 1.75 g.

Carbon Dots CD2 were synthesized via microwave-assisted post-functionalization (amidation) of CD1. Specifically, 0.50 g of CD1 was dissolved in 5 mL of DMF, and a fresh DMF solution of PEI (0.10 g in 5 mL) was added. The mixture was divided into four 5 mL Biotage microwave reaction vials, which were sealed and microwave-irradiated for 20 minutes at 300 W. After irradiation, the vials were allowed to cool to room temperature, and the contents were combined in a single 50 mL round-bottom flask. The resulting brown residue was separated using size exclusion chromatography (Sephadex G-25). The collected fractions were rotavaped to remove DMF solvent. The residue was collected and dried in a vacuum oven at 50°C for 16 hours. The final material (0.55 g) was not fully soluble in water and was analyzed using solid-state methods.

Dialdehyde Starch (DAS) was synthesized according to a published method by our group.[26] Specifically the method followed was the following: A 5% solution of oven-dried native potato starch (dried at 40°C for 48 hours in a vacuum oven) was initially dispersed in distilled water using a magnetic stirrer. Sodium periodate ($NaIO_4$) was then added to the mixture in a 1:1.65 weight ratio of potato starch to $NaIO_4$. To prevent light-induced decomposition of $NaIO_4$, the reaction vessel was wrapped in several layers of aluminum foil. The reaction was conducted at 35°C for 24 hours. The reaction was eventually quenched by adding acetone and centrifuged for 5 minutes at 5000 rpm. The precipitates were further washed with water and centrifuged at 5000 rpm, first for 5 minutes and then for 10 minutes. This was followed by washing with ethanol and centrifugation for 10 minutes at 5000 rpm to remove any remaining unreacted oxidative agents. The oxidized starch (DAS) was dried in a vacuum oven at 35°C for 48 hours. The as dried samples were used for analysis.

2.3.2.1. CD-DAS conjugates preparations. Different mixtures were prepared prior to ABES measurement. Dialdehyde Starch was dissolved in DMAc and divided in 4 portions. The two carbon dots were added to a Dialdehyde starch solution at 5% concentration relative to starch, then, the solution was heated at 120°C overnight. The reaction between aldehyde present on starch and amines present on CD2 was confirmed by the resulting homogeneous dark brown solution obtained, as CD2 is initially not soluble in DMAC. After testing that solution in ABES, an excess of Hexamethylenediamine was added (4:1, Amine: Aldehyde molar ratio) in order to crosslink DAS. A solution of 70% Hexamethylenediamine was also tested as a reference.

2.3.2.2. Reversibility tests. Samples of veneer were pressed using the ABES for 300s at 160°C with the different adhesives formulated. The bonded veneer was then immersed in different solutions. A first batch of bonded veneer was placed in a water solution at pH 7 and a second batch in a solution at pH 4. The shear strength was measured using ABES after 1 hour and 4 hours of immersion. Experiments were done in triplicates.

2.3.3. Characterization

UV-Vis spectra were recorded on a Varian CARY 1E UV – Vis spectrophotometer at 25 ± 1°C. Each measurement was repeated three times. Fourier-transform infrared spectroscopy: Infrared spectrum were recorded using a Fourier-transform infrared spectrophotometer (Spectrum Two, Perkin-Elmer, Llantrisant, UK) equipped with a Universal Attenuated Total Reflectance diamond. Fluorescence spectra were recorded on a HITACHI F-7000 fluorescence spectrophotometer.

All FTIR spectra were collected at a spectrum resolution of 4 cm^{-1}, with 32 scans from 4000 to 500 cm^{-1}. Thermogravimetric analysis: Thermograms were made with a Mettler-Toledo TGA2 (Mettler Toledo, Greifensee, Switzerland), under nitrogen with a flow rate of 40 mL min^{-1}, using alumina pans. 5 to 10 mg of each sample were put in a standard TGA alumina crucible pan and heated from 30°C to 600°C at a heating rate of 10°C min^{-1}.

The changes in glass transition temperature (Tg) of Carbon Dots and Starch were performed using a DSC analyzer (Mettler Toledo DSC3+ equipment, Columbus, USA). The samples were heated from – 30 to 200°C at a heating rate of 30°C min^{-1} followed by a cooling from 200 to – 30°C at – 20°C.min^{-1} under a nitrogen flow of 10 mL·min^{-1}. This cycle was repeated 3 times and only curves corresponding to the 2^{nd} or 3^{rd} heating were analyzed. Approximately 5 mg of priory oven-dried sample (at 50°C for 24 h) was used for each analysis.

The bond strength of the adhesives was evaluated using lab-shear bonds subjected to tensile loading through the ABES technique (Adhesive Bond Evaluation System, Corvalis., USA). This apparatus enables the assessment of strength development characteristics for various adhesive types in shear mode between two thin veneer pieces. It offers a rapid, cost-effective, and immediate method to characterize various bond-influencing parameters notably the curing speed of adhesives. The device consists of a pressing unit associated with a displacement module enabling to cure and test the adhesion on a single device, as shown in Figure 13. Adhesives were applied to a single side of one beech veneer (20×5 mm^2 overlapping area) using spatula to put approximatively around 20 mg of adhesive. The veneers were then hot-pressed under controlled conditions of temperature and time. The temperature was set to 160°C to enable solvent evaporation and avoid reagent evaporation. After curing, the pressure was released, and the bond was immediately subjected to shear testing. Shear strength was recorded at different pressing time. Each condition was tested with 10 replicates.

X-ray Photoelectron spectroscopy (XPS) X-ray photoelectron spectra of CVD graphene samples were recorded on a Quantum 2000 Scanning ESCA instrument) using a monochromatic Al K-Alpha X-ray (1486.7 eV) excitation source.

The morphology of CDs and DAS-CDs was visualized using an Environmental Scanning Electron Microscope (PhilipsXL-30 ESEM, HITACHI, Japan) at 10 KV, with a spot size of 4.3 using the secondary electrons detector for a magnification of 200 and 1000. Before observation, the samples were coated with gold using a sputter coater (Emitech k550X, Quorum Emitech, England).

3. Concluding remarks

We have developed two variants of carbon dots (CDs) with high hydrogen-bonding and covalent-bonding aptitude, suitable for new bio-based adhesive formulations when combined with dialdehyde starch (DAS). Both hydrothermal and microwave-assisted synthetic approaches were successfully employed. Thermal and physicochemical analyses of the CDs indicate high potential for efficient and safe thermomechanical treatment. The ABES study of combined formulations of DAS and CDs revealed significant influences on curing, with CDs assisting in achieving faster curing than DAS alone. Due to the potential of the CDs to act as crosslinkers in the presence of HMDA (an auxiliary crosslinker) at low concentrations, adhesion is enhanced by the imine network and hydrogen bonding offering additional options for adhesive formulations. Furthermore, we demonstrated that these resins can exhibit reversibility induced by an acidic environment, owing to the acidic hydrolysis of imine covalent bonds formed during the curing of the resins, within one hour of treatment.

Disclosure statement

No potential conflict of interest was reported by the author(s).

References

[1] Heinrich, L. A. Future Opportunities for Bio-Based Adhesives – Advantages Beyond Renewability. *Green Chem.* 2019, *21*(8), 1866–1888. DOI: 10.1039/c8gc03746a.

[2] Eisen, A.; Bussa, M.; Röder, H. A Review of Environmental Assessments of Biobased Against Petrochemical Adhesives. *J. Clean. Prod.* 2020, *277*, 124277. DOI: 10.1016/j.jclepro.2020.124277.

[3] Tenorio-Alfonso, A.; Sánchez, M. C.; Franco, J. M. A Review of the Sustainable Approaches in the Production of Bio-Based Polyurethanes and Their Applications in the Adhesive Field. *J. Polym. Environ.* 2020, *28*(3), 749–774. DOI: 10.1007/s10924-020-01659-1.

[4] Gonçalves, D.; Bordado, J. M.; Marques, A. C.; Galhano dos Santos, R. Non-Formaldehyde, Bio-Based Adhesives for Use in Wood-Based Panel Manufacturing Industry—A Review. *Polymers* 2021, *13*(23), 4086. DOI: 10.3390/polym13234086.

[5] Hemmilä, V.; Adamopoulos, S.; Karlsson, O.; Kumar, A. Development of Sustainable Bio-Adhesives for Engineered Wood Panels – a Review. *RSC Adv.* 2017, *7*(61), 38604–38630. DOI: 10.1039/c7ra06598a.

[6] Arias, A.; Feijoo, G.; Moreira, M. T. New Environmental Approach Based on a Combination of Planetary Boundaries and Life Cycle Assessment in the Wood-Based Bioadhesive Market. *ACS Sustainable Chem. Eng.* 2022, *10*(34), 11257–11272. DOI: 10.1021/acssuschemeng.2c03058.

[7] Ciastowicz, Ż.; Pamuła, R.; Białowiec, A. Utilization of Plant Oils for Sustainable Polyurethane Adhesives: A Review. *Materials* 2024, *17*(8), 1738. DOI: 10.3390/ma17081738.
[8] Zhang, S.; Liu, C.; Su, M.; Zhou, D.; Tao, Z.; Wu, S.; Xiao, L.; Li, Y. Development of Citric Acid-Based Biomaterials for Biomedical Applications. *J. Mater. Chem. B* 2024, *12*(45), 11611–11635. DOI: 10.1039/d4tb01666a.
[9] Pooresmaeil, M.; Javanbakht, S.; Namazi, H.; Shaabani, A. Application or Function of Citric Acid in Drug Delivery Platforms. *Med. Res. Rev.* 2021, *42*(2), 800–849. DOI: 10.1002/med.21864.
[10] Kasprzyk, W.; Świergosz, T.; Romańczyk, P. P.; Feldmann, J.; Stolarczyk, J. K. The Role of Molecular Fluorophores in the Photoluminescence of Carbon Dots Derived from Citric Acid: Current State-Of-The-Art and Future Perspectives. *Nanoscale* 2022, *14*(39), 14368–14384. DOI: 10.1039/d2nr03176k.
[11] Chen, S.; Li, X.; Bai, M.; Shi, S. Q.; Aladejana, J. T.; Cao, J. Oyster-Inspired Carbon Dots-Functionalized Silica and Dialdehyde Chitosan to Fabricate a Soy Protein Adhesive with High Strength, Mildew Resistance, and Long-Term Water Resistance. *Carbohydr. Polym.* 2023, *319*, 121093. DOI: 10.1016/j.carbpol.2023.121093.
[12] Yang, P.; Zhu, Z.; Wang, L.; Shen, A.; Tang, M.; Chen, M. Developing Carbon Dots as Green Modifiers for Improving the Bonding Performance of Low-Molar-Ratio Urea-Formaldehyde Resin. *Int. J. Adhes. Adhes.* 2023, *125*, 103416. DOI: 10.1016/j.ijadhadh.2023.103416.
[13] Samanta, S.; Banerjee, S. L.; Bhattacharya, K.; Singha, N. K. Graphene Quantum Dots-Ornamented Waterborne Epoxy-Based Fluorescent Adhesive via Reversible Addition–Fragmentation Chain Transfer-Mediated Miniemulsion Polymerization: A Potential Material for Art Conservation. *ACS Appl. Mater. Interfaces* 2021, *13*(30), 36307–36319. DOI: 10.1021/acsami.1c08812.
[14] Zhang, L.; Wang, W.; Jin, P.; Sun, Z.; Zhan, Y.; Jiang, B. Reactive Carbon Dots/Polysiloxane Composites Cross-Linked Silicone Resin Adhesives for Stable White LED Constructing. *Compos. Commun.* 2025, *53*, 102172. DOI: 10.1016/j.coco.2024.102172.
[15] Aggarwal, M.; Panigrahi, H.; Kotnees, D. K.; Das, P. Multifunctional Self-Healing Carbon Dot–Gelatin Bioadhesive: Improved Tissue Adhesion with Simultaneous Drug Delivery, Optical Tracking, and Photoactivated Sterilization. *Biomacromolecules* 2024, *25*(5), 3178–3189. DOI: 10.1021/acs.biomac.4c00313.
[16] Jelinek, R. *Carbon Quantum Dots: Synthesis, Properties and Applications*; Springer: Cham, 2017.
[17] Ren, J.; Malfatti, L.; Innocenzi, P. Citric Acid Derived Carbon Dots, the Challenge of Understanding the Synthesis-Structure Relationship. *C* 2020, *7*(1), 2. DOI: 10.3390/c7010002.
[18] Xu, D.; Li, C.; Pizzi, A.; Xi, X.; Wang, Z.; Du, G.; Chen, Z.; Lei, H. Self-Neutralizing Citric Acid–Corn Starch Wood Adhesives. *ACS Sustainable Chem. Eng.* 2024, *12*(35), 13382–13391. DOI: 10.1021/acssuschemeng.4c05590.
[19] Schneider, J.; Reckmeier, C. J.; Xiong, Y.; von Seckendorff, M.; Susha, A. S.; Kasák, P.; Rogach, A. L. Molecular Fluorescence in Citric Acid-Based Carbon Dots. *J. Phys. Chem. C* 2017, *121*(3), 2014–2022. DOI: 10.1021/acs.jpcc.6b12519.
[20] Dhenadhayalan, N.; Lin, K.-C.; Suresh, R.; Ramamurthy, P. Unravelling the Multiple Emissive States in Citric-Acid-Derived Carbon Dots. *J. Phys. Chem. C* 2016, *120*(2), 1252–1261. DOI: 10.1021/acs.jpcc.5b08516.
[21] Vallan, L.; Imahori, H. Citric Acid-Based Carbon Dots and Their Application in Energy Conversion. *ACS Appl. Electron. Mater.* 2022, *4*(9), 4231–4257. DOI: 10.1021/acsaelm.2c01021.

[22] Li, H.; Papadakis, R. Fluorescence Imaging Enhanced by Members of the Graphene Family: A Review. *Fluoresc. Imag. Recent Adv. Appl.* 2023. DOI: 10.5772/intechopen.113228.

[23] Meierhofer, F.; Dissinger, F.; Weigert, F.; Jungclaus, J.; Müller-Caspary, K.; Waldvogel, S. R.; Resch-Genger, U.; Voss, T. Citric Acid Based Carbon Dots with Amine Type Stabilizers: pH-Specific Luminescence and Quantum Yield Characteristics. *J. Phys. Chem. C* 2020, *124*(16), 8894–8904. DOI: 10.1021/acs.jpcc.9b11732.

[24] Ye, Y.; Yang, D.; Chen, H.; Guo, S.; Yang, Q.; Chen, L.; Zhao, H.; Wang, L. A High-Efficiency Corrosion Inhibitor of N-Doped Citric Acid-Based Carbon Dots for Mild Steel in Hydrochloric Acid Environment. *J. Hazard. Mater.* 2020, *381*, 121019. DOI: 10.1016/j.jhazmat.2019.121019.

[25] Mohamad Amini, M. A.; Hashim, R.; Sulaiman, N. S.; Mohamed, M.; Sulaiman, O. Citric Acid-Modified Starch as an Environmentally Friendly Binder for Wood Composite Making. *BioRes* 2020, *15*(2), 4234–4248. DOI: 10.15376/biores.15.2.4234-4248.

[26] Gao, F.; Ma, S.; Li, J.; Dai, K.; Xiao, X.; Zhao, D.; Gong, W. Rational Design of High Quality Citric Acid-Derived Carbon Dots by Selecting Efficient Chemical Structure Motifs. *Carbon* 2017, *112*, 131–141. DOI: 10.1016/j.carbon.2016.10.089.

[27] Song, Y.; Zhu, S.; Zhang, S.; Fu, Y.; Wang, L.; Zhao, X.; Yang, B. Investigation from Chemical Structure to Photoluminescent Mechanism: A Type of Carbon Dots from the Pyrolysis of Citric Acid and an Amine. *J. Mater. Chem. C* 2015, *3*(23), 5976–5984. DOI: 10.1039/c5tc00813a.

[28] Boukhvalov, D. W.; Osipov, Y. V.; Murzalinov, D.; Serikkanov, A.; Bi, H. A Comprehensive Model of Carbon Nanodots with 0.21 Nm Lattice Fringes Patterns. *Carbon* 2024, *225*, 119101. DOI: 10.1016/j.carbon.2024.119101.

[29] Neitzel, N.; Hosseinpourpia, R.; Adamopoulos, S. A Dialdehyde Starch-Based Adhesive for Medium-Density Fiberboards. *BioResources* 2023, *18*(1), 2155–2171. DOI: 10.15376/biores.18.1.2155-2171.

[30] Li, H.; Papadakis, R. Click Chemistry Enabling Covalent and Non-Covalent Modifications of Graphene with (Poly)saccharides. *Polymers* 2020, *13*(1), 142. DOI: 10.3390/polym13010142.

[31] Ederer, J.; Janoš, P.; Ecorchard, P.; Tolasz, J.; Štengl, V.; Beneš, H.; Perchacz, M.; Pop-Georgievski, O. Determination of Amino Groups on Functionalized Graphene Oxide for Polyurethane Nanomaterials: XPS Quantitation Vs. Functional Speciation. *RSC Adv.* 2017, *7*(21), 12464–12473. DOI: 10.1039/c6ra28745j.

[32] Lazar, P.; Mach, R.; Otyepka, M. Spectroscopic Fingerprints of Graphitic, Pyrrolic, Pyridinic, and Chemisorbed Nitrogen in N-Doped Graphene. *J. Phys. Chem. C* 2019, *123*(16), 10695–10702. DOI: 10.1021/acs.jpcc.9b02163.

[33] Siddique, A. B.; Hossain, S. M.; Pramanick, A. K.; Ray, M. Excitation Dependence and Independence of Photoluminescence in Carbon Dots and Graphene Quantum Dots: Insights into the Mechanism of Emission. *Nanoscale* 2021, *13*(39), 16662–16671. DOI: 10.1039/d1nr04301c.

[34] Mondal, M.; Pramanik, S. A Mechanism for Excitation-Dependent Emission from Carbon Nanodots. *Mater. Lett. X.* 2023, *18*, 100195. DOI: 10.1016/j.mlblux.2023.100195.

[35] Mintz, K. J.; Bartoli, M.; Rovere, M.; Zhou, Y.; Hettiarachchi, S. D.; Paudyal, S.; Chen, J.; Domena, J. B.; Liyanage, P. Y.; Sampson, R., et al. A Deep Investigation into the Structure of Carbon Dots. *Carbon.* 2021, *173*, 433–447. DOI: 10.1016/j.carbon.2020.11.017.

[36] Letoffe, A.; Hosseinpourpia, R.; Silveira, V.; Adamopoulos, S. Effect of Fenton Reaction Parameters on the Structure and Properties of Oxidized Wheat Starch. *Carbohydr. Res.* 2024, *542*, 109190. DOI: 10.1016/j.carres.2024.109190.

[37] Yong, H.; Liu, J. Recent Advances on the Preparation Conditions, Structural Characteristics, Physicochemical Properties, Functional Properties and Potential Applications of Dialdehyde Starch: A Review. *Int. J. Biol. Macromol.* 2024, *259*, 129261. DOI: 10.1016/j.ijbiomac.2024.129261.

[38] Chaudhary, V.; Panyoyai, N.; Small, D. M.; Shanks, R. A.; Kasapis, S. Effect of the Glass Transition Temperature on Alpha-Amylase Activity in a Starch Matrix. *Carbohydr. Polym.* 2017, *157*, 1531–1537. DOI: 10.1016/j.carbpol.2016.11.028.

[39] Hosseinpourpia, R.; Echart, A.; Adamopoulos, S.; Gabilondo, N.; Eceiza, A. Modification of Pea Starch and Dextrin Polymers with Isocyanate Functional Groups. *Polymers* 2018, *10*(9), 939. DOI: 10.3390/polym10090939.

[40] Ngafwan, N.; Rasyid, H.; Abood, E. S.; Abdelbasset, W. K.; Al-Shawi, S. G.; Bokov, D.; Jalil, A. T. Study on Novel Fluorescent Carbon Nanomaterials in Food Analysis. *Food Sci. Technol.* 2022, *42*, 42. DOI: 10.1590/fst.37821.

[41] Nezhad-Mokhtari, P.; Arsalani, N.; Ghorbani, M.; Hamishehkar, H. Development of Biocompatible Fluorescent Gelatin Nanocarriers for Cell Imaging and Anticancer Drug Targeting. *J. Mater. Sci.* 2018, *53*(15), 10679–10691. DOI: 10.1007/s10853-018-2371-8.

[42] Andreana, I.; Bincoletto, V.; Manzoli, M.; Rodà, F.; Giarraputo, V.; Milla, P.; Arpicco, S.; Stella, B. Freeze Drying of Polymer Nanoparticles and Liposomes Exploiting Different Saccharide-Based Approaches. *Materials* 2023, *16*(3), 1212. DOI: 10.3390/ma16031212.

[43] Wannous, A.; Milaneh, S.; Said, M.; Atassi, Y. New Approach for Starch Dialdehyde Preparation Using Microwave Irradiation for Removal of Heavy Metal Ions from Water. *SN Appl. Sci.* 2022, *4*(5), 4. DOI: 10.1007/s42452-022-05024-w.

[44] Gurr, J.; Barbu, M. C.; Frühwald, A.; Chaowana, P. The Bond Strength Development of Coconut Wood in Relation to Its Density Variations. *J. Adhes.* 2022, *98*(10), 1520–1533. DOI: 10.1080/00218464.2022.2091437.

[45] Zhang, H.; Su, Z.; Wang, X. Starch-Based Rehealable and Degradable Bioplastic Enabled by Dynamic Imine Chemistry. *ACS Sustainable Chem. Eng.* 2022, *10*(26), 8650–8657. DOI: 10.1021/acssuschemeng.2c02537.